Loss and gain of carbon during char degradation.

Michael I. Bird[a,*], *Anna, V. McBeath*[a], *Philippa L. Ascough*[b], *Vladimir A. Levchenko*[c], *Christopher M. Wurster*[a], *Niels C. Munksgaard*[a,e], *Ronald J. Smernik*[d], *Alan Williams*[c],

[a] College of Science, Technology and Engineering and Centre for Tropical Environmental and Sustainability Science, James Cook University, Cairns, Queensland, 4870, Australia

[b] NERC Radiocarbon Facility, Scottish Universities Environmental Research Centre (SUERC), Scottish Enterprise Technology Park, Rankine Avenue, East Kilbride, G75 0QF, UK

[c] Australian Nuclear Science and Technology Organisation (ANSTO), Kirrawee DC, NSW 2232, Australia

[d] School of Agriculture, Food and Wine, Waite Research Institute, The University of Adelaide, Waite Campus, Urrbrae, SA 5064, Australia

[e] Research Institute for the Environment and Livelihoods, Charles Darwin University, Darwin, Northern Territory, Australia

*Corresponding Author -Telephone: +61-7-4242-1137 Email: Michael.bird@jcu.edu.au

KEYWORDS

Biochar, radiocarbon, carbon-isotope, degradation, carbon sequestration

ABSTRACT

We report results of a study examining controls on the degradation of chars produced at 300, 400 and 500˚C from radiocarbon-free wood, deployed for three years in a humid tropical rainforest soil in north Queensland, Australia. The chars were subjected to four treatments (i) no litter (ii) covered by leaf litter, (iii) covered by limestone chips to alter local pH, and (iv) covered by limestone chips mixed with leaf litter. Radiocarbon, stable isotope and proximate analyses indicate significant ingress of exogenous (environmental) carbon and mineral material, strongly correlated with loss of indigenous (char) carbon from the samples. While indigenous carbon losses over three years were generally <8% for the char produced at 500˚C char under any treatment, chars formed at lower temperatures lost 5-22% of indigenous carbon accompanied by ingress of up to 7.5% modern exogenous carbon. The data provide clear evidence of a direct link between the ingress of exogenous carbon, likely due at least partly to microbial colonisation, and the extent of char decomposition. Failure to account for the ingress of exogenous carbon will lead to a significant under-estimate of the rate of char degradation.

35 1. INTRODUCTION

36 Pyrogenic carbon (PyC; soot, char, black carbon) is the product of incomplete combustion of
37 organic material during biomass burning, controlled pyrolysis (biochar) and fossil fuel
38 consumption. Natural and anthropogenic PyC is pervasively distributed throughout the terrestrial
39 and marine environments, atmosphere and the cryosphere (Bird et al., 2015; Santin et al., 2015).

40 PyC is significant in the global carbon cycle as a potentially recalcitrant form of carbon that is
41 stable in the environment over long timescales (centuries to millennia; Preston and Schmidt, 2006;
42 Zimmerman, 2010; Singh et al., 2012). The environmental stability of PyC has attracted attention as
43 a means of sequestering atmospheric carbon dioxide into the soil in the form of biochar, thereby
44 reducing the global warming impacts of anthropogenic CO_2 emissions (e.g. Jeffrey et al., 2015).
45 While it is clear that a component of PyC exhibits a high degree of resistance to degradation in the
46 environment, it is also clear that there is a PyC 'degradation continuum' (Bird et al., 2015), with the
47 rate of degradation of PyC determined by complex interactions between, at least, the feedstock type
48 and temperature of pyrolysis on the one hand, and the environmental conditions to which the PyC is
49 exposed after production in terms of parameters such as at ambient temperature (Zimmerman et al.,
50 2012), moisture availability and soil type (texture, pH, organic carbon and microbial activity).

51 There is a growing body of evidence that chemical modifications of the surface of the charcoal
52 occur rapidly upon environmental exposure (<1yr) and on longer timescales PyC can undergo
53 significant environmental degradation, (eg. Cheng and Lehmann, 2009; Ascough et al., 2011a,
54 2011b), ultimately leading to virtually complete loss of macroscopic PyC (Bird et al., 1999).
55 Degradation is usually framed in terms of loss of carbon by mineralization and/or dissolution.
56 However, it also appears to be the case that at least in the short term, exogeneous carbon and
57 mineral material can become strongly associated with PyC surfaces and pores (Jaafar et al., 2015a
58 and b; Lehmann et al., 2011). PyC has known ability to adsorb organic compounds from the

environment to varying degrees (e.g. Mohan et al., 2014) and indeed biotic degradation of PyC implies at least an initial addition of exogenous carbon during microbial colonization.

It seems likely that PyC degradation is the result of continual carbon exchange between PyC surfaces and the local environment, leading over time to the mineralization/dissolution of a variable amount of PyC-derived carbon. Elucidating the mechanisms by which degradation occurs and the parameters governing the rates at which degradation occurs remains challenging. Previous studies have attempted to investigate these issues through laboratory incubations (Singh et al., 2012; Kuzyakov et al., 2014), field emplacement and monitoring (Major et al., 2010; Zimmerman et al., 2012) and observation of natural systems using a space for time substitution approach (Cheng et al., 2008, Bird et al., 1999; Cheng and Lehmann, 2009).

Isotope labelling with either stable carbon isotopes or radiocarbon has also been used to separately quantify soil and PyC-derived components in both laboratory incubations and field studies (Singh et al., 2012; Kuzyakov et al., 2014; Sagrilo et al., 2015). This study utilizes both stable and radiogenic carbon isotope labelling and a mass balance approach to separately quantify indigenous (char) carbon loss from degradation, and exogenous (environmental) carbon gain from active colonization by soil (micro)biota or passive sorption, through a three-year field deployment of laboratory-produced, radiocarbon-free char on the soil surface of a humid tropical rainforest. Treatments with and without litter, to provide a range in labile carbon supply and limestone chips, to provide a range of local pH conditions, were applied to determine the degree to which priming by labile carbon and/or local pH exert an influence on degradation behaviour. Preliminary radiocarbon results from these samples after one year of environmental exposure have been previously presented (Bird et al., 2014), focusing on the ability of pre-treatment techniques to decontaminate the char for radiocarbon dating.

2. MATERIALS AND METHODS

2.1. Samples

A c.8 million year old log (*Nothofagus* spp.; 10kg) was obtained from the upper 10m of the 70m thick Yallourn brown coal seam in Victoria, Australia. The log was dried at 105˚C, chipped and sieved, with the >2mm fraction retained for pyrolysis. Previous ^{13}C NMR analysis of the wood demonstrated that the material was dominated by lignocellulosic components similar to fresh wood (Bird et al., 2014). Aliquots of the wood (~100g) were pyrolysed under a 3.5 L min^{-1} flow of nitrogen at 305, 414 or 512˚C for 1 hour, using the system described in detail by Bird et al. (2011). The resulting char was lightly crushed and sieved to yield approximately 100g each of the 0.5-2mm fraction for each char. The pyrolysis conditions were chosen to represent a typical range of common temperatures at which char is produced (McBeath et al., 2013) and thereby a range of physico-chemical characteristics in the resultant char that can be expected to influence subsequent colonization by microorganisms and degradation processes (Ascough et al., 2010).

2.2. Field deployment

The site used for these trials was located at the James Cook University Daintree Rainforest Observatory, Cape Tribulation, Queensland (16.103˚S; 145.447˚E; 70m asl). This site was chosen because numerous soil and atmospheric parameters are routinely monitored, and the site is in a hot (mean monthly temperature ranging from 22˚-28˚C; mean annual temperature 25˚C), humid (3,500mm annual rainfall, with a pronounced wet season from December to March) rainforest environment where interactions between char and environment can be expected to be comparatively rapid. This humid tropical forest site has not burned in historical times, and it is likely that natural char abundance in the soil is very low.

Vegetation at the site is an evergreen mesophyll to notophyll vine ‘tall forest’ (Torello-Raventos et al., 2013) that produces abundant broadleaf litter throughout the year. This accumulates to a depth

of 5-10cm in the 'dry' season, decaying away over a period of a few months after the onset of the wet season. The soil is an Acidic, Dystrophic, Brown Dermosol (Isbell 1996) or a Haplic Cambisol (Hyperdystic, Alumic, Skeletic) based on the World Reference Base soil classification (Deckers et al., 1998), developed on colluvium derived from metamorphic and granitic mountains to the west of the site. The upper A-horizon is dark greyish brown silty loam to silty clay loam with many (20-50%) cobbles and stones throughout the profile. The <2mm faction of the soil (0-10cm) is 28% clay, 54% silt and 19% sand, mildly acid (pH 5.5-6.5) and relatively organic-rich (3.7% C, 0.3% N).

Approximately 5 g aliquots of each char type were weighed into triplicate 125 μm aperture nylon mesh bags. The litter bags were pegged to the soil surface and subjected to one of the following four treatments:

(i) NL – all litter removed from the surface and aliquots laid directly on the soil surface;

(ii) L – as for NL but aliquots then covered with a ~5cm thick layer of local leaf litter replenished each six months;

(iii) NL-LM – as for NL but aliquots then covered with a ~5cm thick layer of limestone chips (sieved at 2-10 mm);

(iv) L-LM – as for NL but aliquots covered with a layer of limestone chips (sieved at 2-10 mm) mixed with an equal volume of periodically replenished local leaf litter each six months. A volume of litter equivalent to that applied to L was re-mixed with the limestone chips each six months.

The samples were emplaced in June 2009 and recovered in July 2010 (1 year) and August 2012 (3 years). The area where the samples were emplaced was covered with polyester shade cloth and enclosed in a wire mesh cage to exclude disturbance by foraging wildlife. The purpose of the

limestone chips was to increase local pH, as alkaline conditions have been shown to be a significant determinant of PyC degradation behaviour (Braadbaart et al., 2009; Huismann et al., 2012). Determination of the exact pH experienced by the samples is not possible, but analysis of surface soil and leachate water at the end of the experiment suggests the treatments without limestone addition (L and NL) experienced a local pH between 5.6 and 6.5, while the limestone treatments (L-LM and NL-LM) experienced local pH between 6.6 and 8.0. Upon recovery, the samples were returned to the laboratory, removed from the mesh bags, gently washed free of loosely adhering soil particles, dried at 80˚C and weighed.

2.3. Laboratory analysis

2.3.1. Characterization

Total organic carbon abundance and isotope composition of samples were determined using a Costech elemental analyzer fitted with a zero-blank auto-sampler coupled via a ConFloIV to a ThermoFinnigan DeltaV^{PLUS} using continuous-flow isotope ratio mass spectrometry (EA-CF-IRMS) at James Cook University's Cairns Analytical Unit. Stable isotope results are reported as per mil (‰) deviations from the VPDB reference standard scale for $\delta^{13}C$ values. Precision (standard deviation) on internal standards was better than ±0.1‰. Repeated measurements on samples showed that C concentrations were generally reproducible to ±1% (1σ). The mineral ash content of the samples was determined by loss on ignition at 1020˚C under air, with a multiple replicate measurement precision of ±0.5% (1σ). pH was measured on suspensions of 1g char in 20ml of deionized water after shaking for 1.5 hours (Rajkovich et al., 2012).

Hydrogen pyrolysis (hypy) was used to determine the stable polycyclic aromatic carbon (SPAC) content of the samples, presumed to be resistant to degradation on long timescales (Bird et al., 2015; McBeath et al., 2015). The analysis of PyC by hypy has been described in detail in a number of publications (Meredith et al., 2012 Wurster et al., 2012; McBeath et al., 2015). Briefly, solid ~10-50mg samples were loaded with a Mo catalyst (~10% ofsample mass) using an

aqueous/methanol solution of ammonium dioxydithiomolybdate [$(NH_4)_2MoO_2S_2$]. The dried catalyst-loaded samples were placed in the hypy reactor and pressurized to 150 bar of hydrogen gas with a sweep gas flow of 5 L min^{-1}, then heated at 300 °C min^{-1} to 250 °C, then 8°C min^{-1} until a final hold temperature of 550 °C which was maintained for 2 minutes. The carbon content of the sample before and after hypy was used to calculate PyC content as a fraction of total organic carbon (hereafter stable polycyclic aromatic carbon; SPAC) with an error of ±5% (McBeath et al., 2015).

For determination of radiocarbon activity a 2-3.5mg aliquot of each dried char sample, with no pretreatment, was combusted to CO_2 using the sealed-tube technique and then converted to graphite using the H_2/Fe method (Hua et al., 2001). AMS ^{14}C measurements were carried out using the STAR facility at ANSTO (Fink et al., 2004), which is routinely capable of 0.3% (1σ) precision on modern samples. Raw measurement results were corrected for possible contamination in processing using the standard ANSTO blank correction procedure (see Bird et al., 2014 for further discussion). All results are reported as percent modern carbon (pMC) and as conventional radiocarbon ages following the conventions of Stuiver and Polach (1977).

Solid state ^{13}C cross polarization (CP) NMR spectra were obtained for one aliquot of each of the three initial chars, and one aliquot of each of the same chars after three years environmental exposure to the NL treatment. Spectra were obtained at a frequency of 100.6 MHz using a Varian Unity INOVA400 NMR spectrometer. Samples were packed in 7 mm diameter cylindrical zirconia rotors with Kel-F rotor end caps and spun at the ‘‘magic angle’’ (54.7°) at 6500 ± 100 Hz in a Doty Scientific supersonic MAS probe. Free induction decays (FIDs) were acquired with a sweep width of 50 kHz; 1216 data points were collected over an acquisition time of 160 ms. All spectra were zero filled to 8192 data points and processed with a 50 Hz Lorentzian line broadening and a 0.010 s Gaussian broadening.

Chemical shifts were externally referenced to the methyl resonance of hexamethylbenzene at 17.36 ppm. The spectra represent the accumulation of 4000 scans and were acquired using a 90° ^{1}H pulse

of 5-6 μs duration time, a 1 ms contact time and a 1 s recycle delay. Quantification of the different C species was determined by a deconvolution method as previously described in McBeath et al. (2011). Briefly the deconvolution method involves fitting each spectrum as the sum of multiple peaks of Gaussian shape that have been assigned to the different C regions as determined by the chemical shifts.

Samples for examination by scanning electron microscopy were mounted on aluminium stubs and gold coated before viewing in a JEOL JSM 6300 operating at 10kV. Images were obtained with Semaphore imaging software (JEOL).

2.3.2. Short-term *in vitro* mineralization and $\delta^{13}C$ value of respired CO_2

Aliquots of dried char (≈ 80mg each), after environmental exposure for three years were placed on a wet pre-combusted quartz sand bed (≈ 750mg) in 12mL capacity Exetainer vials sealed with a septum cap for incubation in the dark at 25^{o}C over 7 days, with no applied nutrient source and no inoculum. Milli-Q^{tm} grade water, filtered at 0.2 microns and UV sterilized was added to the combusted sand. The wet sand base provided a stable source of moisture available by capillary action without saturating the samples over the course of the experiment. No inoculum was added as the purpose was to measure the response of any indigenous microbial population in relation to the labile carbon supply inferred to exist based on the radiocarbon measurements.

Two empty vials and two vials with wet sand only were included as blanks. The volumetric concentration and $\delta^{13}C$ values of the evolved CO_2 were measured after 1, 3 and 7 days of incubation using Wavelength-Scanned Cavity Ring-down Spectrometry (Picarro G2131-i). Vial gases were extracted and supplied to the spectrometer via a syringe penetrating the vial septum with simultaneous entry of CO_2-free air via a second syringe. This procedure allowed for sufficient O_2 to be present for respiration throughout the incubation period.

The Picarro G2131-i records CO_2 concentration and $\delta^{13}C$ values at approximately 1 Hz. Integrated CO_2 and $\delta^{13}C$ values over the ≈ 2-5 min analysis time (dependent on CO_2 concentration) were derived using an in-house Excel™ calculation template. The integration window was selected to include all data sets with CO_2 >40 ppm vol. Calibration of concentration values were carried out by analysis of CO_2-free air and a certified CO_2-in-air standard gas (1050 ppm vol) and $\delta^{13}C$ values were calibrated to the VPDB scale by analysing CO_2 evolved from two in-house carbonate standards ($\delta^{13}C$ = -4.67‰, -24.23‰) tied to the certified reference materials NBS-18 and NBS-19. Results are presented as the cumulative totals of the three measurement periods for each aliquot.

2.3.3. Mass balance

Changes in both sample mass and carbon mass can be accurately determined through combination of the re-measured mass and measurement of the carbon content of each aliquot before and after emplacement. As the radiocarbon content of all three starting char samples is indistinguishable from background levels (<0.01 pMC Table 1; Bird et al., 2014), the radiocarbon activity of a sample after field deployment provides a direct measure of partitioning between indigenous carbon and modern exogenous carbon (leaf litter; 106.2±0.4 pMC; 1σ: Bird et al., 2014) in each sample, and this can then also be used to calculate the amount of indigenous carbon lost from each sample from the start (T0) and end (T1) of the field deployment. All masses in the calculations below are in grams (g)

The initial total mass of carbon in an aliquot prior to field deployment (TC_{T0}), where (M_{T0}) is the total mass of the aliquot and $\%C_{T0}$ is the carbon content of the aliquot in percent, is given by:

$$(TC_{T0}) = (M_{T0}) \times \%C_{T0} \quad \text{--- equation 1}$$

The proportional change in aliquot mass between the mass deployed (M_{T0}) and that remaining after a environmental exposure (M_{T1}), is given by:

$$\% \text{ change} = [(M_{T0} - M_{T1}) / M_{T0}] * 100 \quad \text{--- equation 2}$$

227 The mass of total carbon (TC_{T1}) after environmental exposure, is calculated from the mass of an
228 aliquot remaining at T1 and its total carbon content in percent ($\%C_{T1}$):

229 $TC_{T1} = M_{T1} \times \%C_{T1}$ --- equation 2

230 The mass of exogenous carbon that has been added to an aliquot as a result of environmental
231 exposure (EC_{T1}) is determined directly from the radiocarbon activity (in percent Modern Carbon;
232 pMC) of the sample after environmental exposure (pMC_{T1}):

233 $EC_{T1} = TC_{T1} \times pMC_{T1}$ --- equation 3

234 The mass of indigenous carbon that remains in an aliquot after environmental exposure (IC_{T1}) is
235 then obtained by difference:

236 $IC_{T1} = TC_{T1} - EC_{T1}$ --- equation 4

237 The proportional loss of indigenous carbon over the period of environmental exposure can then be
238 calculated from the mass difference between total carbon in an aliquot prior to exposure and
239 indigenous carbon remaining in the same aliquot after environmental exposure:

240 $\%\ change = [(TC_{T0} - IC_{T1}) / TC_{T0}] * 100$ --- equation 5

241 The stable carbon-isotope composition of three starting chars ($\delta^{13}Ci$) was determined to be -21.1‰
242 (300 ˚C), -21.4‰ (400 ˚C) and -21.5‰ (500 ˚C) all with an analytical uncertainty of ±0.1‰. These
243 $\delta^{13}C$ values are distinct from the measured $\delta^{13}C$ values of the two likely exogenous carbon sources
244 ($\delta^{13}C_e$) that ranged from leaf litter at the site (-29.0‰) to limestone chips (>-2‰). The $\delta^{13}C$ value
245 of each sample after environmental exposure ($\delta^{13}C_{T1}$) was obtained to test competing hypotheses
246 for exogenous carbon origin, through an isotope mass balance of the form:

247 $\delta^{13}C_{T1} = (\delta^{13}C_e \times F_e) + (\delta^{13}C_i \times (1-F_e)))$ --- equation 6

where F_e is the proportion of carbon in a sample after environmental exposure that is exogenous, and is equivalent to the radiocarbon activity in percent modern carbon divided by 100.

All treatments were deployed and analyzed in duplicate, but for simplicity of presentation, data are presented as means plus or minus the deviation of duplicates from the mean.

253 3. RESULTS

254 The characteristics of the chars prior to deployment are provided in Table 1 and the full data set for
255 all samples is presented in Table S1.

256 Initial ash content is low (<1%) and the radiocarbon (^{14}C) content is negligible for all samples
257 before deployment. Carbon content (63.7 to 76.9%) and pH (4.7-5.6) increases and $\delta^{13}C$ values (-
258 21.1 to -21.5‰) decrease with increasing temperature of formation, all generally consistent with
259 results from other thermosequence studies (e.g. Rajkovich et al., 2012; Wurster et al., 2015). The
260 proportion of recalcitrant carbon (SPAC) increases from 5.7% of TOC to 59% of TOC with
261 increasing temperature, implying a decrease in the amount of labile and semi-labile carbon for the
262 higher temperature chars, also consistent with other studies (Bird et al., 2015).

263 Several coherent trends are evident in all samples over the course of the trial, with details dependent
264 both on the temperature of formation of the char and the treatment applied in the field. After one
265 year, the mass of char deployed increased due to the incorporation of a variable amount of mineral
266 material and exogenous carbon (Figure 1A). This increase of up to ~30-35% in mass was
267 particularly marked in the lower temperature chars with no litter (NL), although increases in mass
268 and carbon of <10% were observed in all samples. The increase in mass is mirrored by an increase
269 in radiocarbon activity (for those samples analysed after 1 year), with higher activities of ~0.5-
270 1pMC recorded by the NL chars regardless of production temperature, but increases of <0.3 pMC
271 recorded by all other chars analysed (Figure 1B). Likewise, the $\delta^{13}C$ values of all chars decreased
272 marginally, by up to 0.25‰ (Figure 1C).

273 Mass balance calculations (equation 4) assuming that exogenous carbon has a $\delta^{13}C$ value similar to
274 modern leaf litter at the site (-29.0‰) suggests a consistency between the observed increase in
275 radiocarbon activities and the observed decrease in $\delta^{13}C$ values. For example a 5-10% contribution
276 of exogenous carbon to the 300˚C char should lead to a decrease in $\delta^{13}C$ value of 0.4-0.8‰ while a

277 1-2% input of exogenous carbon into the 500˚C char should lead to a decrease in $\delta^{13}C$ value of 0.1-
278 0.2‰. Note that the loss of indigenous carbon could lead to muting of the observed decrease in $\delta^{13}C$
279 values as 'semi-labile' carbon in C_3 wood chars has been shown to be depleted in ^{13}C relative to the
280 bulk char by ~1‰ up to 500˚(Wurster et al., 2015). Loss of this 'semi-labile' component would
281 tend to increase the $\delta^{13}C$ value of the remaining char, thereby partly offsetting the observed
282 decrease in $\delta^{13}C$ values due to exogenous carbon input. The inference of a loss of indigenous
283 carbon is borne out by the relationship shown in Figure 2, which suggests a significant negative
284 correlation (F-ratio 1,22 = 22.8, $p<0.001$) between radiocarbon activity and $\delta^{13}C$ difference. The
285 figure also shows the more limited changes that have occurred in the L-LM and NL-LM treatments
286 compared to the L and NL treatments.

287 Figure 3 shows a significant negative correlation (F-ratio 1,22 = 110.6, $p<0.001$) with decreasing
288 carbon content of the 3-year chars associated with increasing ash content. The figure also shows
289 that the L-LM and NL-LM trends tend to be less modified in composition (lower in ash, higher in
290 C) than the L and NL treatments and the 500˚C chars less modified than the lower temperature
291 chars. Figure 4 indicates that over the three years, all samples lost indigenous carbon, with the
292 500˚C chars losing the least amount (2-8%), while lower temperature chars lost 5-22% of carbon
293 originally present in the sample. Generally, the L and NL lower temperature chars lost more
294 indigenous carbon than the equivalent chars in the L-LM and NL-LM treatments. Figure 4 also
295 demonstrates a significant correlation (F-ratio 1,22 = 33.47, $p<0.001$) between the loss of
296 indigenous carbon and the ingress of exogenous carbon as marked by increased radiocarbon
297 activity.

298 Imaging of the char surfaces by scanning electron microscopy demonstrates the presence of
299 adhering mineral material and fungal hyphae to varying degrees in all samples (see Figure 5 for the
300 NL treatment), consistent with the observed increases in ash content due to adhesion of soil
301 material, and with the observed increase in radiocarbon activity.

302 Solid-state ^{13}C cross polarization (CP) NMR spectroscopy was used to examine the molecular
303 changes within the chars after 3 years of environmental exposure for samples from the NL
304 treatment. The NMR spectra for representative aliquots from the NL treatment are presented in
305 Figure 5. Changes in the molecular structure of the original char thermosequences has been
306 described previously in Bird et al. (2014). Briefly, there is clear progression in the composition of
307 the char structure with increasing temperature (from 300°C to 500°C) where the lignocellulosic
308 structure of the starting material breaks down leading to the progressive development of aromatic
309 structures. The ^{13}C CP NMR spectrum of the 300°C char is dominated by resonances of
310 lignocellulosic materials that have not completely thermally degraded. By 400°C the majority of
311 this lignocellulosic material is lost and the spectrum becomes dominated by an aryl peak at 130ppm
312 and an O-aryl shoulder at 150ppm. There is evidence of some residual alkyl C (broad peak at
313 30ppm) that is presumably due to the formation of relatively resistant alkyl structures produced at
314 lower temperatures. By 500˚C the spectrum is dominated by aryl-C.

315 The most apparent changes between the original chars over the 3 years were observed for the 300°C
316 NL char where there was a 1.5% loss in N-alkyl and methoxyl groups and a 1.1% loss in O-Aryl
317 groups. There is also an increase of 2.5% in O-alkyl groups. The 400°C NL char spectra are broadly
318 similar between the original and environmentally exposed biochar, as was also observed after one
319 year of exposure (Bird et al., 2014). The 500°C NL char, despite having the greatest proportion of
320 relatively stable aromatic C, lost aryl and O-aryl groups in the amount of 4.5% and 1.1%
321 respectively, alongside an increase in O-alkyl groups of 4.5%.

322 Cumulative CO_2 respired from the samples after drying and laboratory rewetting ranged from 24 to
323 76 μmol CO_2 g^{-1}, with a median deviation from the mean of replicate aliquots of ±2 μmol CO_2 g^{-1}.
324 The lowest amounts of CO_2 were respired from the 500˚C chars and the highest by the 300˚C chars,
325 irrespective of treatment (Figure 6a). A tendency for higher amounts of respired CO_2 to be
326 associated with samples that experienced more indigenous carbon loss at each temperature was not

significant. The $\delta^{13}C$ value of the respired CO_2 ranged widely from -28.4 to -20.6‰, approximating the range between the litter and char end-member isotope compositions, with a median deviation from the mean of replicate aliquots of ±0.5‰. The $\delta^{13}C$ value was closely related to temperature of formation and, for the 300˚ and 400˚C chars, also correlated with indigenous carbon loss (Figure 6b) and therefore with radiocarbon activity (Figure 4).

4. DISCUSSION

The data presented in this study provide the first clear evidence of a direct link between the ingress of exogenous carbon and the extent of char decomposition. The increase in ash content, which is highest in the NL treatment, is likely simply the result of the passive introduction of soil mineral material from processes such as rainsplash and the movement of small (<125μm) soil fauna although some authigenic mineral formation on char surfaces cannot be ruled out. The relationship between ash content and carbon content (Figure 3) could also simply be interpreted as the passive accumulation of exogenous organic carbon from local litter and soil on char surfaces, and it is likely that some of the carbon does derive from mineral-associated carbon, adsorbed dissolved organic carbon and/or fine particulate carbon. However, the strong relationship between the amount of exogenous carbon (measured by radiocarbon and $\delta^{13}C$ value; Figures 2 and 4) and the amount of indigenous carbon lost over the three years implies an active role for the exogenous microbial carbon, possibly augmented or facilitated by organo-mineral interactions, in promoting indigenous carbon loss. It is also likely that the accumulation of mineral matter adhering to the char to the extent that it was not removed by gentle washing of the samples (see methods) was facilitated by microbial mucilage, such that the greater the degree of microbial colonization, the higher the final ash content of the samples.

The amount of carbon lost through degradation is lowest in the 500 ˚C chars and generally highest in the 300 ˚C chars, for each treatment type. This further supports the conclusion that carbon loss is dominantly driven by microbial colonization and utilization of the chars, with the degree to which the char-derived carbon is susceptible to loss through microbial respiration or solubilisation being driven by the proportions of labile, semi-labile and recalcitrant carbon (*sensu* Bird et al., 2015) present in the chars. The amount of semi-labile and recalcitrant carbon is in turn determined by temperature of formation.

357 The relationships between loss of indigenous carbon, respired CO_2 and the $\delta^{13}C$ value of the
358 respired CO_2 further support an active role for microbes in the degradation process (Figure 6). Any
359 readily labile indigenous carbon in the chars would have been lost over the three years of
360 environmental exposure. The pulse of CO_2 from all samples decreased by a factor of three to four
361 over the course of the week-long incubation. This indicates a small pool of very labile carbon that
362 was rapidly respired upon rewetting of the samples in the laboratory, derived from microbial
363 biomass killed by drying at 80 ˚C at the end of the field deployment, and potentially also labile
364 environmental carbon from litter or soil. This pool of carbon is highest in the 300˚C chars and
365 lowest in the 500˚C chars, consistent with the lower temperature chars being better able to support a
366 microbial population.

367 The $\delta^{13}C$ value of respired CO_2 is ~2‰ lower than the $\delta^{13}C$ value of the substrate being respired by
368 a microbial population (Santruckova et al., 2000). In this experiment all sources of exogenous
369 carbon were derived from a C_3 source with an average $\delta^{13}C$ value of -29‰. Some components of
370 this exogenous carbon (e.g. cellulose) could be 1-2‰ higher in $\delta^{13}C$ value than the bulk litter
371 (Benner et al., 1987), but values above ~-27‰ in this study can be confidently ascribed to carbon
372 originally derived from the chars (~-21‰), present in the samples as dead microbial biomass,
373 readily respirable by a reinvigorated microbial population upon rewetting and incubation. Values
374 above -29‰ are likely to contain some component of char-derived carbon but less confidence can
375 be ascribed to this conclusion. 70% of all measurements are >-27‰ indicating a contribution to the
376 respired CO_2 from the char, including all but two of the 300 ˚C and 400 ˚C char aliquots; all
377 respired CO_2 samples have $\delta^{13}C$ values >-29‰. Very high $\delta^{13}C$ values, close to the $\delta^{13}C$ values of
378 the chars were observed in the limestone treatments (NL-LM and L-LM) of the 300 ˚C samples and
379 at all temperatures the limestone treatments tended to higher $\delta^{13}C$ values than the non-limestone
380 treatment; observations that are discussed further below.

381 Several characteristics of the physico-chemical evolution and degradation behaviour of the chars
382 are similar to previously reported results. After one year, all samples showed a significant increase
383 in mass due to the adhesion of mineral soil particles, consistent with other studies (Jaafar et al.,
384 2015a and b), and there was a measurable increase in modern exogenous carbon (as determined by
385 both ^{14}C and ^{13}C), consistent with the observation of fungal hyphae in the samples (Bird et al.,
386 2014) and also reported by direct observation in other studies (Ascough et al., 2009; Lehmann et al.,
387 2011; Jaafar et al., 2015a and b). There was a further increase in mass after three years,
388 accompanied by an increase in associated mineral material, evident in a variably elevated ash
389 content in all samples up to 35% (Figure 3).

390 A relationship between the susceptibility of alteration of chars and temperature of char formation
391 has also been reported (e.g. Singh et al., 2012; Ascough et al., 2011a; McBeath et al., 2015). In this
392 study, the 500 ˚C char universally showed the least modification of any properties over time
393 consistent with the high proportion of largely inert SPAC (59% of TOC) in this char, while the 300
394 ˚C char generally, but not universally, showed the most significant change over time, consistent
395 with the low proportion of SPAC (5.7% of TOC).

396 Decomposition rates cannot be calculated for these chars in this experiment because there are
397 insufficient time steps, and more importantly because the chars are likely composed of components
398 with multiple turnover times potentially ranging from months to millennia (Bird et al., 2015). The
399 observed loss of indigenous carbon over the three years of 14-20% for the 300 and 400 ˚C chars in
400 the L and NL treatments, coupled with the low SPAC contents of these chars (Table 1), does imply
401 the likelihood of essentially complete degradation to gaseous or solubilized forms over a few
402 decades at most, in this humid tropical environment. This conclusion is consistent with other studies
403 that have shown comparatively rapid loss of char produced at relatively low temperatures on annual
404 to decadal timescales (Bird et al. 1999; Knicker et al., 2013; Sagrilo et al., 2015). The lower losses
405 of 5-8% for the 500 ˚C in the L and NL treatments confirm that these chars are comparatively
406 resistant to decomposition, with the comparatively high radiocarbon of some of the chars (~4 pMC)

implying microbial colonization of the chars but with lower ability to use the carbon in the chars as a metabolic substrate.

While the limestone (L-LM and NL-LM) treatments exhibited the same general trends with regard to the temperature of char formation, the comparatively low degree of alteration of all the limestone treatments compared to no limestone treatments (L and NL) was not expected. Previous research has clearly demonstrated that alkaline conditions lead to enhanced degradation of char particles in laboratory experiments and archaeological sites (Bradbaart et al., 2009; Huisman et al., 2012). The absence of an enhanced degradation effect due to pH may be due to the comparatively small change in pH conditions in this study (from ~6 to ~8) for the surface soil, compared to pH values up to 12 for recently-formed wood and peat ash commonly associated with char in archaeological sites (Braadbaart et al., 2009). However, these observations do not explain why the limestone treatments in general led to less apparent alteration of the chars, with less ingress of exogenous carbon, even when litter was added with the limestone.

The possibility that radiocarbon-free dissolved carbon in the form of carbonate from the limestone chips was incorporated into the chars in the L-LM and NL-LM treatments cannot be absolutely discounted. However, using equation 4 and assuming the lowest realistic $\delta^{13}C$ value of -2‰ for this limestone component suggests that the measured $\delta^{13}C$ value of, for example, the 300 ˚C chars should have *increased* by 1-2‰ if a limestone-derived carbon component was present in the quantities (5-10% of total carbon; Figure 4 and Table S1) required to 'mask' the loss of radiocarbon-free indigenous carbon, if indigenous carbon was actually lost to the same degree (15-22% of total carbon; Figure 4 and Table S1) as the L and NL treatments. The observed much lower ingress of mineral material in the limestone treatments, in tandem with the lower ingress of exogenous carbon into the limestone-treated samples also argues against the likelihood of a significant limestone-derived carbon component in the samples.

For each temperature of char formation, the degree of alteration as measured by ash content, indigenous carbon loss and isotope composition, generally decreased in the order NL>L>NL-LM~L-LM. This suggests that oxygen availability may have played a role in promoting degradation, with cover either by litter or by limestone chips potentially reducing oxygen availability at the char surface. During the wet season, the soil is usually wet to water-logged and the 5cm layer of litter applied to the L treatment potentially led to waterlogging for a longer duration than the NL samples, thereby reducing oxygen availability to the L samples to a greater degree than the NL samples. Limestone cover associated with the LM treatments likely further physically reduced the ability of oxygen to penetrate to the char surfaces, particularly during the wet season, compared to L treatment where there was no cover by litter or limestone.

The suggestion that oxygen availability is a driver of degradation rate must be considered speculative, as the possibility could not be tested *post hoc*. However, if this were the case, then it has implications for PyC degradation in the broader environment as it would suggest that degradation is likely to proceed more rapidly in coarse-textured more porous soils than in finer-textured soils – a conclusion that does have some observational support (e.g. Sagrilo et al., 2015). It further suggests that, where water is not limiting, degradation may proceed faster on the soil surface than at depth in the soil, a conclusion that also has some observational support (Zimmerman et al., 2012).

While it is possible that the change in pH in the limestone treatments may have made the local environment less amenable to microbial colonization, as the chars themselves are acidic (Table 1), the field observation of fungal hyphae beneath the limestone chips suggests that pH itself was not a major determinant of degradation rate. However a further possibility is that Ca^{2+} released by the reaction of lime chips with the slightly acidic soil and rainfall was primarily responsible for the effects seen in the LM treatments. Oades (1988) summarised the various influences on organic matter retention in soils and identified that high concentrations of Ca^{2+} tend to decrease organic matter solubilisation and mobility. Importantly in the context of the current study, this would also

457 restrict the mobility of both organic matter and inorganic colloids. Decreased mobility of degraded
458 carbon is consistent with the lower apparent loss of char carbon, the lower apparent ingress of non-
459 char carbon into the char particles and the lower apparent ingress of inorganic material into the char
460 particles for the LM treatments.

461 Such an interpretation is also consistent with the comparatively high $\delta^{13}C$ values of respired CO_2
462 for the limestone treatments that approached the $\delta^{13}C$ values of the chars themselves in some cases,
463 and were generally higher than the no limestone treatments (Figure 6). This suggests that
464 indigenous carbon is being degraded, and rendered potential labile and mobile, but not being
465 mobilized and lost from the char. Hence this degraded indigenous carbon was available for
466 respiration when the samples were rewetted in the laboratory in the absence of limestone cover and
467 in the presence of oxygen. While the inferred effect of Ca^{2+} must also be considered speculative, as
468 it was not possible to test this possibility *post hoc*, the retarding influence of Ca^{2+} on organic matter
469 mobility has been established in numerous situations ranging from tundra soils (Wittinghall and
470 Hobbie, 2012) to temperate pastures (Varcoe et al., 2010).

471 If increased Ca^{2+} concentration does retard the loss of degradation products, this may partly explain
472 why char from alkaline environments - with alkaline conditions often the result of proximity to
473 limestone - is often susceptible to large losses of carbon during the alkali pre-treatment step of the
474 conventional AAA (acid-alkali-acid) pre-treatment for radiocarbon dating (Bradbaart et al., 2009;
475 Bird et al., 1999; 2014). It may be the case that char degradation products, which would otherwise
476 be removed by leaching after their formation in the absence of Ca^{2+}, are simply immobilized *in situ*
477 by Ca^{2+} bridging, are not leached away, and are therefore available to then be removed by the alkali
478 (generally NaOH) step of the AAA pre-treatment.

479 In conclusion, this study has clearly demonstrated that the loss of indigenous carbon as a result of
480 environmental degradation is offset to a variable degree by the ingress of carbon from the
481 environment, from both the passive accumulation of mobilized soil/litter-derived carbon and active

482 microbial colonization. The study demonstrates the exogenous carbon added to the char can
483 represent a substantial fraction (up to a third) of the indigenous carbon lost through degradation
484 after only three years. Failure to account for the addition of exogenous carbon is likely to lead to a
485 significant under-estimate of the rate of degradation of char, where this is quantified using a mass
486 balance approach. The study clearly suggests that temperature of formation is the dominant control
487 on degradation rate and that degradation is closely linked to microbial activity. Factors such as
488 oxygen availability and Ca^{2+} availability may also play a subordinate role, with further research
489 required to substantiate these possibilities.

490 5. ACKNOWLEDGMENTS

491 We thank Mr. William Wood of True Energy Pty Ltd for provision of the wood sample used in this
492 study, Mr Andrew Jenkinson for performing the radiocarbon measurements on the STAR
493 accelerator and the members of the AMS radiocarbon chemistry team for processing this study's
494 samples through to accelerator cathodes. This project was supported by an Australian Research
495 Council Federation Fellowship (FF0883221) to MIB, AINSE grant ALNGRA10061 to MIB and
496 VL and National Environmental Research Council (UK) Standard Grant number, NE/F017456/1 to
497 MIB and PLA.

498 6. REFERENCES

499 Ascough, P. L.; Bird, M. I.; Meredith, W.; Snape, C. E.; Vane, C.; Brock, F.; Higham, T.
500 Hydropyrolysis as a tool for enhanced ^{14}C age measurement and quantification of Black Carbon in
501 depositional environments. *Quaternary Geochronology*, **2009**, *4*, 140-147.

502 Ascough, P.L.; Bird, M.I.; Meredith, W.; Wood, R.E.; Snape, C.E.; Brock, F.; Higham, T.F.G.;
503 Large, D.; Apperley, D. Hydropyrolysis: Implications for radiocarbon pre-treatment and
504 characterization of Black Carbon. *Radiocarbon*, **2010a**, *52*, 1336-1350.

505 Ascough, P.; Sturrock, C. J.; Bird, M. I. Investigation of growth responses in saprophytic fungi to
506 charred biomass. *Isotopes in Environmental and Health Studies*, **2010b**, *46*, 64-77 doi:
507 10.1080/10256010903388436.

508 Ascough P.L.; Bird M.I.; Francis S.M.; Thornton, B.; Midwood, A.J.; Scott, A.C.; Apperley, D.
509 Variability in oxidative degradation of charcoal: influence of production conditions and
510 environmental exposure. *Geochimica et Cosmochimica Acta*, **2011a**, *75*, 2361-2378. DOI:
511 10.1016/j.gca.2011.02.002

512 Ascough P. L.; Bird, M. I.; Francis, S. M.; Lebl, T. Alkali extraction of archaeological and
513 geological charcoal: Evidence for diagenetic degradation and formation of humic acids. *Journal of*
514 *Archaeological Science*, **2011b**, *38*, 69-78 doi:10.1016/j.jas.2010.08.011

515 Benner, R.; Fogel, M. L.; Sprague, E. K.; Hodson, R. E.; Depletion of 13 C in lignin and its
516 implications for stable carbon isotope studies. *Nature*, **1987**, *329*(6141), 708-710.

517 Bird, M.I.; Ayliffe, L.K.; Fifield, K.; Cresswell, R.; Turney, C. Radiocarbon dating of 'old'
518 charcoal using a wet oxidation - stepped combustion procedure. *Radiocarbon*, **1999**, *41*, 127-140.

519 Bird, M. I.; Moyo, C.; Veenendaal, E. M.; Lloyd, J.; Frost, P. Stability of elemental carbon in a
520 savanna soil. *Global Biogeochemical Cycles*, **1999**, *134*, 923-932.

521 Bird, M.I.; Wurster, C.W.; de Paula Silva, P.H.; Bass, A.; de Nys, R. Algal Biochar – Production
522 and Properties. *Bioresource Technology*, **2011**, *102*, 1886-1891.
523 doi:10.1016/j.biortech.2010.07.106

524 Bird, M.I.; Ascough, P.L. Isotopes in pyrogenic carbon: a review. *Organic Geochemistry*, **2012**,
525 *42*, 1529-1539.

526 Bird, M. I.; Levchenko, V.; Ascough, P. L.; Meredith, W.; Wurster, C. M.; Williams, A.; Tilston,
527 E.L.; Snape, C.E.; Apperley, D. C. The efficiency of charcoal decontamination for radiocarbon
528 dating by three pre-treatments–ABOX, ABA and hypy. *Quaternary Geochronology*, **2014**, *22*, 25-
529 32.

530 Bird, M. I.; Wynn, J. G.; Saiz, G.; Wurster, C. M.; McBeath, A. The pyrogenic carbon cycle.
531 *Annual Reviews of Earth Planetary Sciences*, **2015**, *43*, 9-1.

532 Braadbaart, F.; Poole, I.; Van Brussel, A. A. Preservation potential of charcoal in alkaline
533 environments: an experimental approach and implications for the archaeological record. *Journal of*
534 *Archaeological Science*, **2009**, *368*, 1672-1679.

535 Cheng, C.-H.; J. Lehmann, J.; Thies, J.E.; Burton, S.D. Stability of black carbon in soils across a
536 climatic gradient. *Journal of Geophysical Research*, **2008**, *113*, G02027,
537 doi:10.1029/2007JG000642.

538 Cheng, C.H.; Lehmann, J. Ageing of black carbon along a temperature gradient. *Chemosphere*,
539 **2009**, *75*, 1021-1027.

540 Deckers, J. A.; Nachtergaele, F.; Spaargaren, O. C.; *World reference base for soil resources:*
541 *Introduction* (Vol. 1). **1998**, Acco.

542 Fink, D.; Hotchkis, M.; Hua, Q.; Jacobsen, G.; Smith, A. M.; Zoppi, U.; Child, D.; Mifsud, C.;
543 van der Gaast, H.; Williams, A.; Williams, M. The ANTARES AMS facility at ANSTO. *Nucl.*
544 *Instrum. Methods Phys. Res.; Sect. B*, **2004**, *224*, 109–115. doi:10.1016/j.nimb.2004.04.025.

545 Hua, Q.; Jacobsen, G. E.; Zoppi, U.; Lawson, E. M.; Williams, A. A.; Smith, A. M.; McGann,
546 M.J.; Progress in radiocarbon target preparation at the ANTARES AMS centre. *Radiocarbon*, **2001**,
547 *432A*, 275–282.

548 Huisman, D. J.; Braadbaart, F.; van Wijk, I. M.; van Os, B. J. H. Ashes to ashes, charcoal to dust:
549 micromorphological evidence for ash-induced disintegration of charcoal in Early Neolithic LBK
550 soil features in Elsloo The Netherlands. *Journal of Archaeological Science*, **2012**, *39*4, 994-1004.

551 Isbell, R.; *The Australian soil classification*. *Revised Edition (Volume 4).* CSIRO publishing,
552 **2002**, 145pp.

553 Jaafar, N. M.; Clode, P. L.; Abbott, L. K. Soil Microbial Responses to Biochars Varying in
554 Particle Size, Surface and Pore Properties. Pedosphere, **2015a**, *255*, 770-780.

555 Jaafar, N. M.; Clode, P. L.; Abbott, L. K.. Biochar-Soil Interactions in Four Agricultural Soils.
556 *Pedosphere*, **2015b***, 255*, 729-736.

557 Jeffery, S.; Bezemer, T. M.; Cornelissen, G.; Kuyper, T. W.; Lehmann, J.; Mommer, L.;
558 Groenigen, J. W. The way forward in biochar research: targeting trade- offs between the potential
559 wins. *GCB Bioenergy*, **2015**, *71*, 1-13.

560 Knicker, H.; González-Vila, F. J.; González-Vázquez, R. Biodegradability of organic matter in
561 fire-affected mineral soils of Southern Spain. *Soil Biology and Biochemistry*, **2013**, *56*, 31-39.

562 Kuzyakov, Y.; Bogomolova, I.; Glaser, B. Biochar stability in soil: Decomposition during eight
563 years and transformation as assessed by compound-specific ^{14}C analysis. *Soil Biology and*
564 *Biochemistry*, **2014**, *70*, 229-236.

565 Lehmann, J.; Rillig, M. C.; Thies, J.; Masiello, C. A.; Hockaday, W. C.; Crowley, D. Biochar
566 effects on soil biota–a review. *Soil Biology and Biochemistry*, **2011**, *439*, 1812-1836.

567 Major, J.; Lehmann, J.; Rondon, M.; Goodale, C. Fate of soil- applied black carbon: downward
568 migration, leaching and soil respiration. *Global Change Biology*, **2010**, *164*, 1366-1379.

569 McBeath, A. V.; Smernik, R. J.; Schneider, M. P.; Schmidt, M. W.; Plant, E. L. Determination of
570 the aromaticity and the degree of aromatic condensation of a thermosequence of wood charcoal
571 using NMR. *Organic Geochemistry*, **2011**, *42*(10), 1194-1202.

572 McBeath, A. V.; Smernik, R. J.; Krull, E. A demonstration of the high variability of chars
573 produced from wood in bushfires. *Organic Geochemistry*, **2013**, *55*, 38-44.

574 McBeath, A. V.; Wurster, C. M.; Bird, M. I. Influence of feedstock properties and pyrolysis
575 conditions on biochar carbon stability as determined by hydrogen pyrolysis. *Biomass and*
576 *Bioenergy*, **2015**, *73*, 155-173.

577 Meredith, W.; Ascough, P.L.A.; Bird, M.I.; Large, D.J.; Snape, C.E.; Yongge Sun, Y. and Tilston,
578 E.L. Assessment of hydropyrolysis as a method for the quantification of black carbon using
579 standard reference materials. *Geochim. Cosmochim Acta,* **2012**, *97*, 131-147.

580 Mohan, D.; Sarswat, A.; Ok, Y. S.; Pittman, C. U.; Organic and inorganic contaminants removal
581 from water with biochar, a renewable, low cost and sustainable adsorbent–a critical review.
582 *Bioresource technology*, **2014**, *160*, 191-202.

583 Oades J.M. (1988) The retention of organic matter in soils. *Biogeochemistry*, **1988**, *5*, 35–70.

584 Preston, C. M.; Schmidt, M. W. I. Black pyrogenic carbon: a synthesis of current knowledge and
585 uncertainties with special consideration of boreal regions. *Biogeosciences*, **2006**, *34*, 397-420.

586 Rajkovich, S.; Enders, A.; Hanley, K.; Hyland, C.; Zimmerman, A. R.; Lehmann, J.; Corn growth
587 and nitrogen nutrition after additions of biochars with varying properties to a temperate soil.
588 *Biology and Fertility of Soils*, **2012**, *48*(3), 271-284.

589 Sagrilo, E.; Rittl, T. F.; Hoffland, E.; Alves, B. J.; Mehl, H. U.; Kuyper, T. W. Rapid
590 decomposition of traditionally produced biochar in an Oxisol under savannah in Northeastern
591 Brazil. *Geoderma Regional*, **2015**, *6*, 1-6.

592 Santín, C.; Doerr, S. H.; Kane, E. S.; Masiello, C. A.; Ohlson, M.; la Rosa, J. M.; ... & Dittmar, T.
593 Towards a global assessment of pyrogenic carbon from vegetation fires. *Global Change Biology*.
594 **2015**, doi: 10.1111/gcb.12985

595 Šantrůčková, H.; Bird, M. I.; Lloyd, J. Microbial processes and carbon- isotope fractionation in
596 tropical and temperate grassland soils. *Functional Ecology*, **2000,** *14*(1), 108-114.

597 Singh, B. P.; Cowie, A. L.; Smernik, R. J. Biochar carbon stability in a clayey soil as a function of
598 feedstock and pyrolysis temperature. *Environmental Science and Technology*, **2012**, *4621*, 11770-
599 11778.

600 Stuiver, M.; Polach, H.A. Discussion: reporting of ^{14}C data. *Radiocarbon*, **1977**, *19*, 355–63.

601 Torello-Raventos M, et al. On the delineation of tropical vegetation types with an emphasis on
602 forest/savanna transitions. *Plant Ecology and Diversity,* **2013**, 6, 101–137.

603 Varcoe, J.; van Leeuwen, J.A.; Chittleborough, D.J.; Cox, J.W.; Smernik, R.J. and Heitz, A.
604 Changes in water quality following gypsum application to catchment soils of the Mount Lofty
605 Ranges, South Australia. *Organic Geochemistry*, **2010**, *41*(2), 116-123.

606 Whittinghill, K.A. and Hobbie, S.E. Effects of pH and calcium on soil organic matter dynamics in
607 Alaskan tundra. *Biogeochemistry*, **2012**, *111*(1-3), 569-581.

608 Wurster, C.M.; Lloyd, J.; Goodrick, I.; Saiz, G. and Bird, M.I. Quantifying the abundance and
609 stable isotope composition of pyrogenic carbon using hydrogen pyrolysis. *Rapid Commun. Mass*
610 *Spectrom*. **2012**, *26*, 2690–2696. DOI: 10.1002/rcm.6397

611 Wurster, C.M.; Saiz, G.; Schneider, M.; Schmidt, M.W.I.; Bird, M.I. Quantifying pyrogenic
612 carbon from thermosequences of wood and grass using hydrogen pyrolysis. *Organic Geochemistry,*
613 **2013**, *62*, 28-32.

614 Wurster, C. M.; McBeath, A. V.; Bird, M. I. The carbon isotope composition of semi-labile and
615 stable pyrogenic carbon in a thermosequence of C_3- and C_4-derived char. *Organic Geochemistry*,
616 **2015**, *81*, 20-26.

617 Zimmerman, A. R. Abiotic and microbial oxidation of laboratory-produced black carbon biochar.
618 *Environmental Science and Technology*, **2010**, *444*, 1295-1301.

619 Zimmermann, M.; Bird, M. I.; Wurster, C.; Saiz, G.; Goodrick, I.; Barta, J.; Capek, P.;
620 Santruckova, H.; Smernik, R. Rapid degradation of pyrogenic carbon. *Global Change Biology*,
621 **2012**, *18*(11), 3306-3316.

622

623

624 **Table 1.** Characteristics of the three chars used in this study (carbon content and radiocarbon data
625 reproduced from Bird et al., 2014). Note TOC = total organic carbon, SPAC = stable polycyclic
626 aromatic carbon. EC = Electrical Conductivity.

ID	Temp. (˚C)	Ash (%)	TOC (%)	pH	^{14}C pMC	$\delta^{13}C$ (‰)	SPAC (% of TOC)
300	305	0.74	63.7	4.7	<0.01	-21.1	5.7
400	414	0.67	71.2	4.5	<0.01	-21.4	50.0
500	512	0.58	76.9	5.6	<0.01	-21.5	59.0

627
628
629

630 **Figure Captions**

631 **Figure 1.** Change in char characteristics after one and three years field deployment. NL = no litter;
632 L = litter; NL-LM = no litter plus limestone chips; L-LM = litter plus limestone chips (see text for
633 further details). Errors are deviations from the mean of separate duplicate aliquots of char deployed
634 under the same treatment, processed separately in the laboratory. Positive values = increase,
635 negative values = decrease.

636 **Figure 2.** Relationship between radiocarbon activity and difference between the $\delta^{13}C$ value of the
637 original char and char after three years deployment. 300˚C and 500 ˚C chars from each of the four
638 treatments indicated. NL = no litter; L = litter; NL-LM = no litter plus limestone chips; L-LM =
639 litter plus limestone chips (see text for further details). Errors are deviations from the mean of
640 separate duplicate aliquots of char deployed under the same treatment, processed separately in the
641 laboratory.

642 **Figure 3.** Relationship between ash content and carbon content of all chars after three years
643 deployment. 300˚C and 500˚C chars from each of the four treatments indicated. See figure 2 for
644 further explanation.

645 **Figure 4.** Relationship between radiocarbon activity and the loss of indigenous carbon for all chars
646 after deployment on a humid tropical rainforest soil surface for three years. 300˚C and 500˚C chars
647 from each of the four treatments indicated. Indigenous carbon loss was calculated as the apparent
648 total carbon loss plus the amount of exogenous carbon as determined by radiocarbon activity. See
649 figure 2 for further explanation.

650 **Figure 5.** SEM images of the 300, 400 and 500˚C chars from the NL (no litter treatment) after three
651 years of environmental exposure, and NMR scans of the same chars prior to deployment and after
652 three years of exposure, with estimates of proportion of major functional groups (see text). Spinning
653 side-bands indicated by an arrow. Comparable SEM images of the 500˚C char prior to field
654 emplacement and after one year in the field have been presented in Bird et al. (2014), and SEM

655 examination of the 300˚C and 400˚C chars prior to emplacement revealed no features other than
656 those observed in the 500˚C char. There were no clear differences in the images of chars from the
657 other treatments to those presented here.

658 **Figure 5.** Relationship between (A) CO_2 respired from an aliquot of each sample over 7 days in the
659 laboratory (B) the $\delta^{13}C$ value of the respired CO_2 and the loss of indigenous carbon after three
660 years. Regressions provided for the 300˚, 400˚ and 500˚C sets of chars. The regressions in (A) are
661 not significant, the regression for the 500˚C chars in (B) is not significant, but is for 400˚C (slope =
662 -0.151, intercept = - 23.7, $r^2 = 0.46$, $p = 0.064$); 300˚C (slope = -0.353, intercept = - 19.6, $r^2 =$
663 0.87, $p < 0.001$).

664

Figure 1. Change in char characteristics after one and three years field deployment. NL = no litter; L = litter; NL-LM = no litter plus limestone chips; L-LM = litter plus limestone chips (see text for further details). Errors are deviations from the mean of separate duplicate aliquots of char deployed under the same treatment, processed separately in the laboratory. Positive values = increase, negative values = decrease.

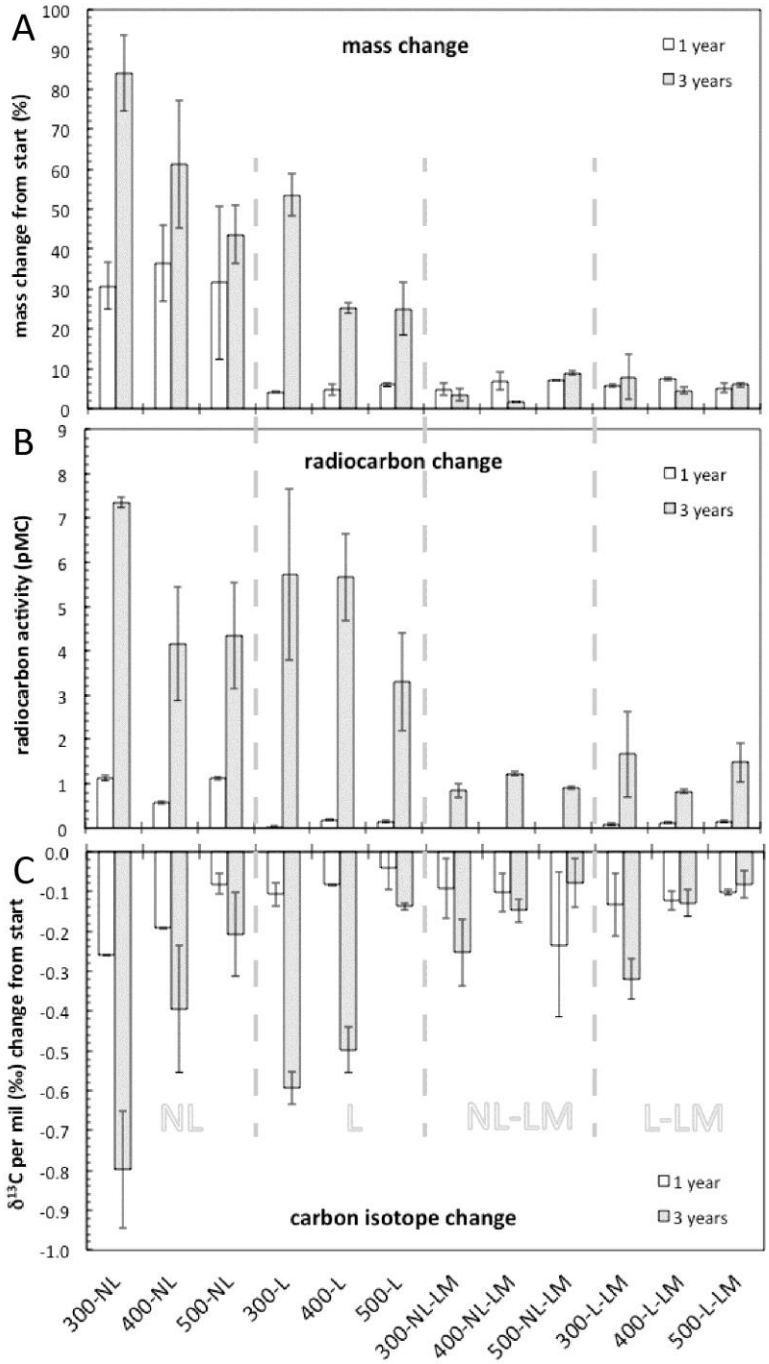

672 **Figure 2.** Relationship between radiocarbon activity and difference between the $\delta^{13}C$ value of the
673 original char and char after three years deployment. 300˚C and 500 ˚C chars from each of the four
674 treatments indicated. NL = no litter; L = litter; NL-LM = no litter plus limestone chips; L-LM =
675 litter plus limestone chips (see text for further details). Errors are deviations from the mean of
676 separate duplicate aliquots of char deployed under the same treatment, processed separately in the
677 laboratory.

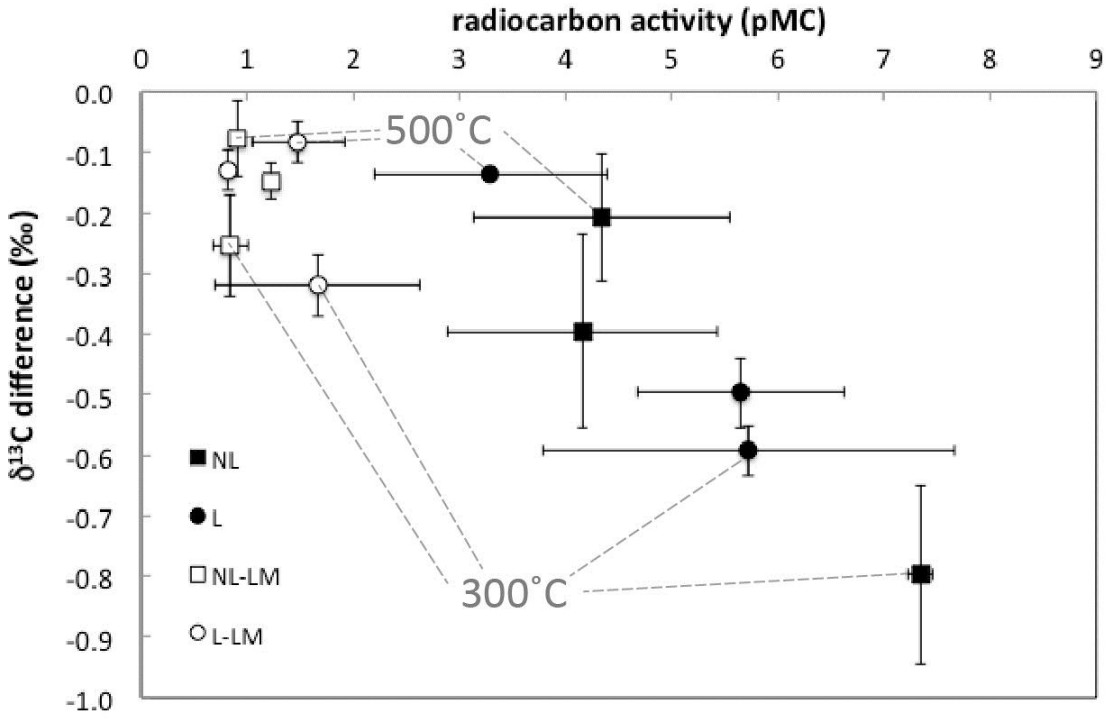

678
679
680

Figure 3. Relationship between ash content and carbon content of all chars after three years deployment. 300˚C and 500˚C chars from each of the four treatments indicated. See figure 2 for further explanation.

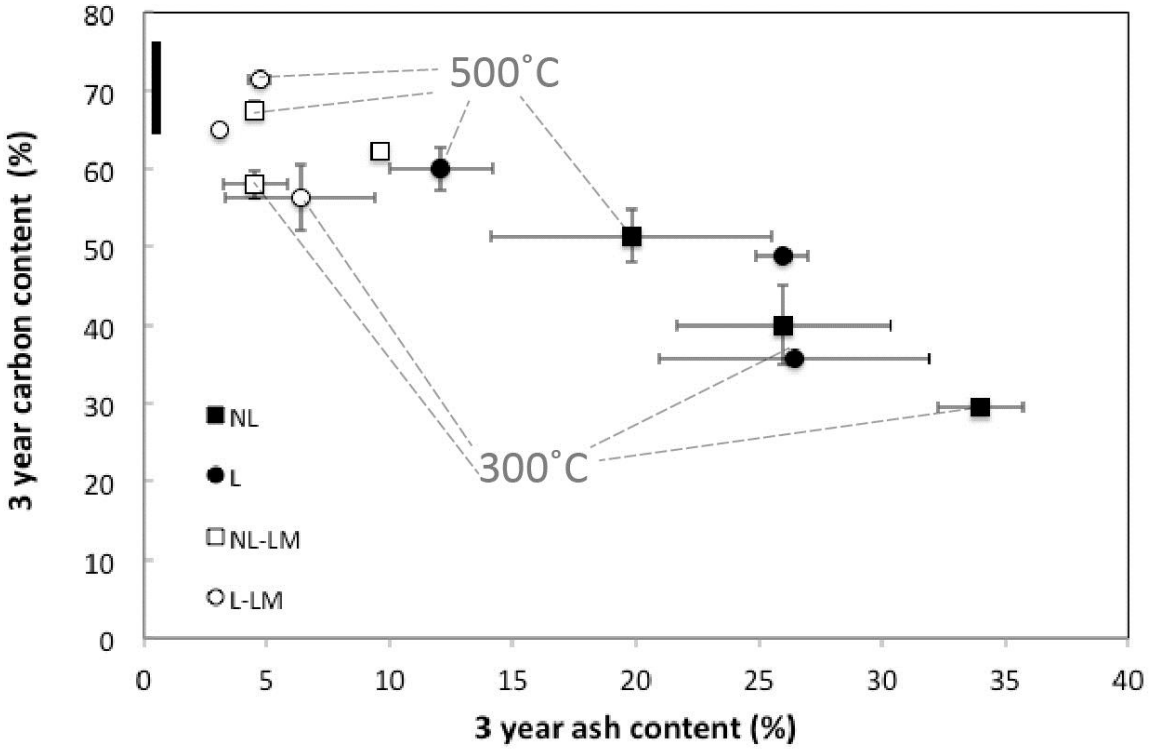

687 **Figure 4.** Relationship between radiocarbon activity and the loss of indigenous carbon for all chars
688 after deployment on a humid tropical rainforest soil surface for three years. 300˚C and 500˚C chars
689 from each of the four treatments indicated. Indigenous carbon loss was calculated as the apparent
690 total carbon loss plus the amount of exogenous carbon as determined by radiocarbon activity. See
691 figure 2 for further explanation.

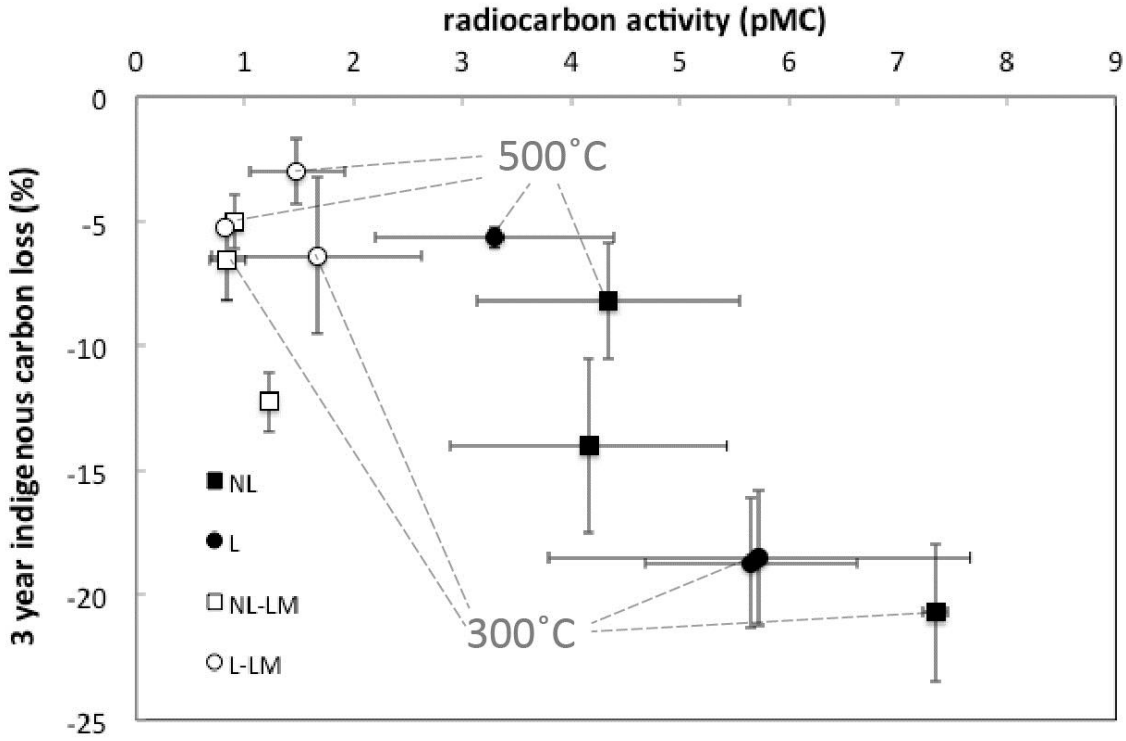

692

693

694

695 **Figure 5.** SEM images of the 300, 400 and 500˚C chars from the NL (no litter treatment) after three
696 years of environmental exposure, and NMR scans of the same chars prior to deployment and after
697 three years of exposure, with estimates of proportion of major functional groups (see text). Spinning
698 side-bands indicated by an arrow. Comparable SEM images of the 500˚C char prior to field
699 emplacement and after one year in the field have been presented in Bird et al. (2014), and SEM
700 examination of the 300˚C and 400˚C chars prior to emplacement revealed no features other than
701 those observed in the 500˚C char.

220µm
300°C
180µm
400°C
140µm
500°C
after three years exposure
initial material
PPM
percent
300 original
300 treatment NL
400 original
400 treatment NL
500 original
500 treatment NL
Alkyl
N-Alkyl/Methoxyl
O-Alkyl
Aryl
O-Aryl

702

Figure 6. Relationship between (A) CO_2 respired from an aliquot of each sample over 7 days in the laboratory (B) the $\delta^{13}C$ value of the respired CO_2 and the loss of indigenous carbon after three years. Regressions provided for the 300˚, 400˚ and 500˚C sets of chars. The regressions in (A) are not significant, the regression for the 500˚C chars in (B) is not significant, but is for 400˚C, p = 0.067; 300˚C p <0.001.

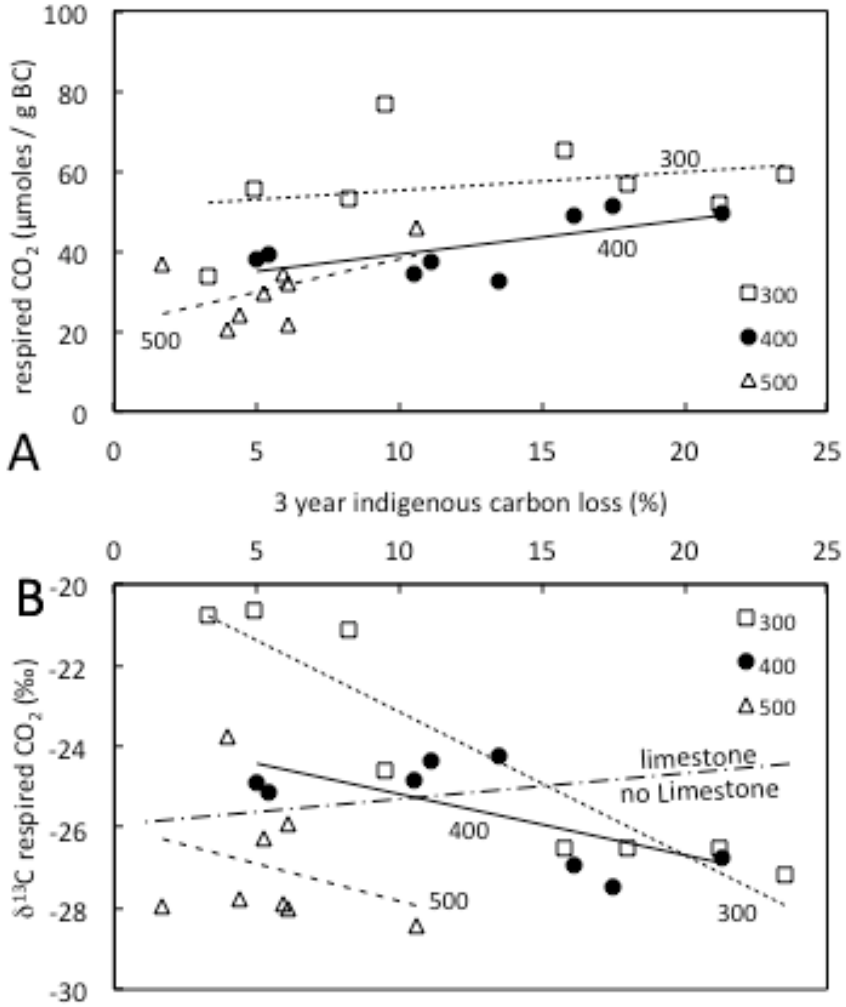

Table S1: Isotope and chemical data for all samples. 'ID' is pyrolysis temperature followed by the treatment applied during field deployment. 'Mass change' is increase in total mass of each aliquot; 'ash' is the mineral component; 'C' is total organic carbon content; 'C change' is increase or decrease (-) in the amount of indigenous carbon, after correction for the ingress of exogenous carbon using radiocarbon activity; $\delta^{13}C$ is the carbon isotope composition of total organic carbon; 'ANSTO ID' is the radiocarbon analysis identifier and ^{14}C is the measured radiocarbon activity; '7 day resp CO_2' is the cumulative amount of CO_2 respired over seven day, 'resp CO_2 $\delta^{13}C$' is the carbon isotope composition of the CO_2. One-year results from Bird et al. (2014).

ID	one year				three year									
	mass change	ANSTO ID	^{14}C	error	mass change	ash	C	C change	$\delta^{13}C$	ANSTO ID	^{14}C	error	7 day resp CO_2	resp CO_2 $\delta^{13}C$
	(%)	OZN-	pMC		(%)	(%)	(%)	(%)	(‰)	OZP-	pMC		(µmol/g)	(‰)
300-NL	36.6	086	1.12	0.05	74.6	32.3	29.9	-23.5	-21.7	450	7.23	0.08	59.0	-27.2
300-NL	24.9				93.6	35.7	29.0	-18.0	-22.0	451	7.46	0.08	56.5	-26.5
300-L	4.1	087	0.03	0.02	58.7	31.9	36.4	-15.8	-21.7	452	7.66	0.09	65.5	-26.5
300-L	4.4				48.2	20.9	35.1	-21.2	-21.7	453	3.79	0.06	52.2	-26.5
300-L-LM	6.5				5.1	5.9	56.2	-8.2	-21.4	454	1.01	0.05	53.4	-21.2
300-L-LM	3.3				2.0	3.2	59.8	-4.9	-21.3	455	0.68	0.03	55.8	-20.7
300-NL-LM	5.5	088	0.08	0.02	13.6	9.4	52.0	-9.5	-21.5	456	2.63	0.06	76.6	-24.6
300-NL-LM	6.1				2.3	3.3	60.6	-3.3	-21.4	457	0.70	0.03	33.9	-20.8
400-NL	26.9	089	0.58	0.03	77.3	30.3	34.9	-17.5	-21.6	442	5.43	0.07	51.6	-27.4
400-NL	45.8				45.2	21.6	45.1	-10.5	-22.0	443	2.88	0.05	34.6	-24.8
400-L	3.3	090	0.19	0.02	23.9	27.0	48.2	-21.3	-21.8	444	6.63	0.08	49.2	-26.7
400-L	6.1				26.4	24.9	49.4	-16.1	-22.0	445	4.68	0.06	48.8	-26.9
400-L-LM	4.8				1.6	9.7	61.3	-13.5	-21.6	446	1.17	0.07	32.3	-24.2
400-L-LM	9.1				1.7	9.5	63.0	-11.1	-21.5	447	1.27	0.04	37.6	-24.3
400-NL-LM	7.1	091	0.12	0.02	3.7	3.2	65.7	-5.0	-21.6	448	0.87	0.04	38.1	-24.9
400-NL-LM	7.7				5.4	3.0	64.4	-5.4	-21.5	449	0.78	0.03	39.3	-25.1
500-NL	50.8	092	1.12	0.04	51.0	25.5	48.0	-10.6	-21.6	458	5.55	0.07	46.0	-28.4
500-NL	12.4				36.3	14.1	54.7	-5.9	-21.8	459	3.14	0.06	34.6	-27.9
500-L	6.4	093	0.15	0.03	31.5	14.2	57.3	-6.1	-21.6	460	4.40	0.07	31.9	-28.0
500-L	5.6				18.5	10.0	62.8	-5.2	-21.6	461	2.19	0.05	29.4	-26.3
500-L-LM	7.1				9.7	4.6	66.4	-6.1	-21.5	462	0.93	0.05	21.7	-25.9
500-L-LM	7.0				8.4	4.4	68.7	-4.0	-21.6	463	0.88	0.03	20.4	-23.7
500-NL-LM	4.0	094	0.16	0.03	6.6	5.2	72.2	-1.7	-21.6	464	1.92	0.04	36.9	-27.9
500-NL-LM	6.5				5.4	4.3	70.5	-4.4	-21.5	465	1.04	0.04	24.2	-27.8

720